SISSA

PAPER • OPEN ACCESS

Beam delivery and final focus systems for multi-TeV advanced linear colliders

View the article online for updates and enhancements.

ICFA BEAM DYNAMICS NEWSLETTER#83 —
CHALLENGES IN ADVANCED ACCELERATOR CONCEPTS

Beam delivery and final focus systems for multi-TeV advanced linear colliders

G. White,[a,*] **S. Gessner,**[a] **E. Adli,**[b] **G.J. Cao,**[b] **K. Sjobak,**[b] **S. Barber,**[c] **C. Schroeder,**[c] **D. Terzani,**[c] **J. van Tilborg,**[c] **E. Esarey,**[c] **C. Doss,**[d] **M. Litos,**[d] **I. Lobach,**[e] **J. Power**[e] **and C.A. Lindstrøm**[f]

[a]*SLAC National Accelerator Laboratory,*
2575 Sand Hill Road, Menlo Park, CA 94025, U.S.A.

[b]*University of Oslo,*
Problemveien 7, 0315 Oslo, Norway

[c]*Lawrence Berkeley National Laboratory,*
1 Cyclotron Road, Berkeley, CA 94720, U.S.A.

[d]*University of Colorado Boulder,*
Boulder, CO 80309, U.S.A.

[e]*Argonne National Laboratory,*
9700 S Cass Ave, Lemont, IL 60439, U.S.A.

[f]*Deutsches Elektronen-Synchrotron DESY,*
Notkestraße 85, 22607 Hamburg, Germany

E-mail: whitegr@slac.stanford.edu

ABSTRACT: The Beam Delivery System (BDS) is a critical component of a high-energy linear collider. It transports the beam from the accelerator and brings it to a focus at the Interaction Point. The BDS system includes diagnostic sections for measuring the beam energy, emittance, and polarization, as well as collimators for machine protection. The length of the BDS increases with collision energy. Higher collision energies also require higher luminosities, and this is a significant constraint on the design for energy-frontier machines. Here, we review BDS designs based on traditional quadrupole magnets and examine the challenges involved in extending these to the Multi-TeV regime consistent with requirements for advanced accelerator concepts.

---

*Corresponding author.

Contents

1 Introduction

The required functionality of a Beam Delivery System (BDS) for a Multi-TeV, advanced Linear Collider concept has been well explored in more "traditional" designs, in pre-existing facilities and their conceived successors. We describe the functionality of existing designs using the ILC [1] as a guide, and briefly discuss expected challenges when extending to higher energies and other pushed parameters represented by the requirements of these more advanced colliders. We then use CLIC as an example of some of the trade-offs in design required when going to higher energies, and then go on to explore, in a broader sense, how the length of a BDS design can be expected to scale to multi-TeV energies. We then highlight selected topics relevant for extending existing BDS designs into the regime required by these advanced accelerator concepts. Finally, we look at two key physics effects which provide hard limits on BDS performance: the Oide effect and beamstrahlung radiation.

2 Anatomy of a beam delivery system

In the context of a linear collider, the BDS is responsible for transporting the e+/e- beams from the exit of the high energy linacs, focusing them to the sizes required to meet the luminosity goals (vertical beam sizes of order a few nm, horizontal size a few 100 nm for a damping ring source), bringing them into collision, and then transporting the spent beams to the main beam dumps. In addition, the BDS must perform several other critical functions:

- measure the linac beam and match it into the final focus, removing any unwanted residual aberrations (e.g., dispersion and coupling errors);

- protect the beamline and detector against mis-steered beams from the main linacs;

- remove any large amplitude particles (beam-halo) from the linac to minimize background in the detectors;

- measure and monitor the key physics parameters such as energy and polarization before (and after) the collisions

The BDS must also provide sufficient instrumentation, diagnostics and feedback systems to achieve these goals.

The core designs and technologies involved in BDS operation have been under constant development since the first implementation (in the Linear Collider context) with SLC [2] (1989-1998). The current state-of-the-art is represented by the designs, and associated systems tests, developed and performed by the ILC [1] and CLIC [3] collaborations. The ILC design is considered the most mature, with considerable engineering effort in place for considering the operation of the BDS in conjunction with the ILC detectors. The layout of the BDS, showing the various subsystems, is shown below in figure 1. The Twiss parameters representing the beam optics design for the BDS is shown in figure 2. We introduce the various subsystems of the ILC BDS for reference below and then discuss CLIC (see figure 4) and the differences of this design in the following section.
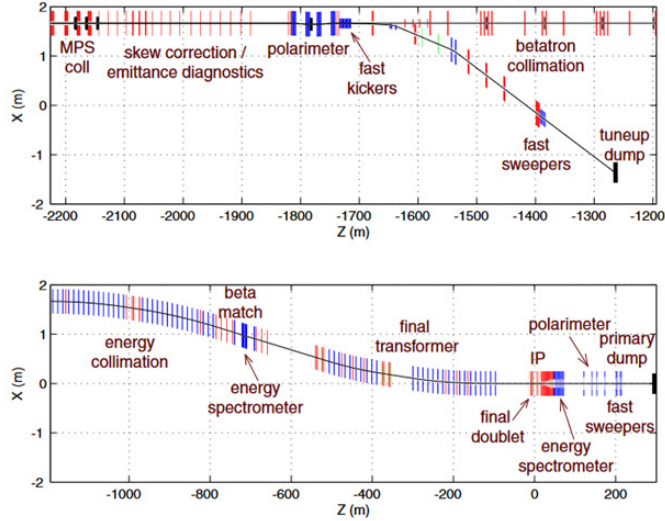
Figure 1. Schematic layout showing ILC BDS subsystems [1].
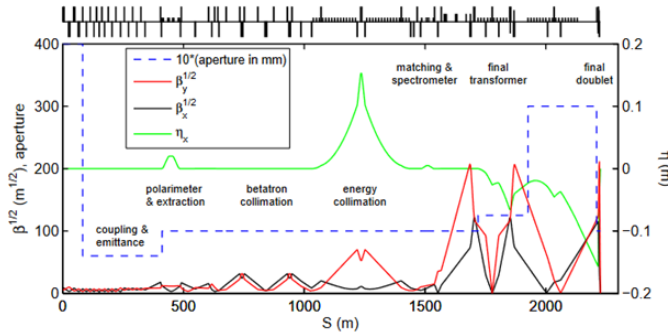
Figure 2. Twiss parameters and beam apertures of the ILC BDS [1].

2.1 Diagnostics, tune-up dump, machine protection

The initial part of the BDS is responsible for measuring and correcting the properties of the beam before it enters the Collimation and Final Focus systems. In addition, errant beams (e.g. bunch centroids significantly offset in position and/or energy beyond the acceptance bandwidth of the BDS) must be detected here and safely extracted in order to protect the downstream systems. Starting at the exit of the main linac, the system includes the MPS collimation system, skew correction section, emittance diagnostic section, polarimeter with energy diagnostics, fast extraction/tuning system and beta matching section.

2.1.1 MPS collimation

At the exit of the main linac is a short 90° FODO lattice, composed of large bore quadrupoles, which contains a set of sacrificial collimators of decreasing aperture. The purpose of this system is to protect the BDS aperture from any beam which develops an extremely large trajectory in the larger aperture main linac. This section also contains kickers and cavity BPMs for inter- and intra-train

trajectory feedback. Acceleration technologies for multi-TeV colliders are likely to have less stable operating parameters than envisioned for ILC and such systems are expected to be of increased importance.

2.1.2 Skew correction

The skew correction section contains 4 orthonormal skew quadrupoles which provide complete and independent control of the 4 betatron coupling parameters (see e.g. [4]). This scheme allows correction of any arbitrary linearized coupled beam. For damping ring sources with large horizontal:vertical emittance ratios, coupling control in the BDS is very important. Future facilities which are based on photo-cathode sources with round beam emittance configurations may be able to save costs by excluding this subsystem.

2.1.3 Emittance diagnostics

The emittance diagnostic section contains 4 "laser wires" which are capable of measuring horizontal and vertical RMS beam sizes down to 1 µm. The wire scanners are separated by 45° in betatron phase to allow a complete measurement of 2D transverse phase space and determination of the projected horizontal and vertical emittances. Use of laser wires is critical to avoid intercepting-style emittance diagnostics, which is of heightened importance as one continues to higher energies.

2.1.4 Polarimeter, laser wire photon and energy diagnostics

Following the emittance diagnostic section are magnetic chicanes which are used for laser wire gamma rays, Compton polarimetry and beam energy diagnostics. At the center of the first chicane is a detector for the Compton-scattered photons from the laser wires, in the second, the Compton IP, and in the last, a BPM for measuring relative beam energy changes, and a sacrificial machine protection system (MPS) energy collimator which defines the energy acceptance of the tune-up extraction line. The length of the chicanes are set to limit horizontal emittance growth due to synchrotron radiation to less than 1%.

Given the limitations on use of chicanes at higher energies, the necessity of some of these devices need to be re-examined by the physics and detector communities when extending into the multi-TeV regime (see later section on energy scaling).

2.1.5 Tune-up and emergency extraction system

A pulsed extraction system is used to extract beams in the event of an intra-train MPS fault. It is also used any time when beams are not desired in the collimation, final focus, or Interaction Region (IR) areas, for example during commissioning of the main linacs. The extraction system includes both fast kickers which can rise to full strength in between bunches, and pulsed bends which can rise to full strength in between trains. These are followed by a transfer line with ±10% momentum acceptance which transports the beam to a full-beam-power water-filled dump.

For advanced multi-TeV designs which may assume a CW pulse structure, the emergency extraction system is somewhat relaxed (other than for the stiffer beam requirements) as the intra-train system is not required. Obviously the beam dump itself becomes more complex at higher beam powers for higher energy beams.

2.2 Collimation system

Particles in the beam halo produce backgrounds in the detector and must be removed in the BDS collimation system. One of the design requirements for the ILC BDS is that no particles are lost in the last several hundred meters of beamline before the IP. Another requirement is that all synchrotron radiation passes cleanly through the IP to the extraction line. The BDS collimation must remove any particles in the beam halo which do not satisfy these criteria. These requirements define a system where the collimators have very narrow gaps and the system is designed to address the resulting machine protection, survivability and beam emittance dilution issues.

The collimation system has a betatron collimation section followed by energy collimators. The downstream energy collimators help to remove the degraded energy particles originating from the betatron collimation section but not absorbed there. The betatron collimation system has two spoiler/absorber x/y pairs located at high beta points, providing single-stage collimation at each of the final doublet (FD) and IP betatron phases. The energy collimation section has a single spoiler located at the central high dispersion point. The betatron spoilers as well as the energy spoiler are "survivable" – they can withstand a hit of two errant bunches of 250 GeV/beam, matching the emergency extraction design goal. With a 500 GeV beam, they would survive only one bunch, and would therefore require more effective MPS or the use of a pre-radiator scheme.

Wakefield calculations for the BDS spoilers and absorbers give IP jitter amplification factors [5] of $A_x = 0.14$ and $A_y = 1.05$. These are scalar amplification factors of relative incoming position jitter: estimated as, $\delta\epsilon/\epsilon = (0.4 n_{jitter} A)^2$, this gives emittance dilutions of 0.08% and 4.4% in the x and y planes respectively, for 0.5 σ incoming beam jitter. Energy jitter at the collimators also amplifies the horizontal jitter at the IP. An energy jitter of 1% produces a horizontal emittance growth of 2.2%.

The halo collimators for advanced accelerators at higher energies are subject to higher power loads due to the increased beam energy and possibly higher halo population due to the presence of interacting material as part of the advanced (e.g. plasma) acceleration devices. It is likely in these cases that the survivable collimator scenario outlined for ILC would not work and that a "renewable" collimation system would need to be developed. Additionally, due to the considerably enhanced beam loading in the advanced accelerating devices, higher levels of beam instability (jitter) may be unavoidable. It is expected in these cases that the wakefields assessed above will become more dominant and must be carefully considered during the collimation system design.

2.3 Muon suppression

Electromagnetic showers created by primary beam particles in the collimators produce penetrating muons which can easily reach the collider hall. The muon flux through the detector is reduced by a 5 m long magnetized iron shield 330 m upstream of the collision point which fills the cross-sectional area of the tunnel and extends 0.6 m beyond the ID of the tunnel. The shield has a magnetic field of 1.5 T, with opposite polarities in the left and right halves of the shield such that the field at the beamline is zero. The shield also provides radiation protection for the collider hall during access periods when beam is present in the linac and beam switch yard.

Higher beam energies and higher halo populations in advanced accelerator concepts will yield higher muon fluxes with more penetration power and careful consideration should be given.

2.4 Halo power handling

The power handling capacity of the collimation system is set by two factors: the ability of the collimators to absorb the incident beam power, and the ability of the muon suppression system to reduce the muon flux through the detector. The muon suppression system presents the more restrictive limitation, setting a tolerance of 1–2×10^{-5} on the fraction of the beam which is collimated in the BDS. Since the actual beam halo conditions are somewhat uncertain, the BDS includes caverns large enough to increase the muon shield from 5 m to 18 m and to add additional toroidal muon spoiler systems. The primary beam spoilers and absorbers are water cooled and capable of absorbing 1×10^{-3} of the beam continuously, which is the maximum expected halo population experience during operations at SLC.

At multi-TeV beam energies, radiated SR power from the various bending systems will also become considerable, damage and further background generation directly from SR losses is not considered a challenge for existing LC designs but should be further considered here.

2.5 Tail-folding octupoles

The final focus includes two (superconducting in the case of ILC) octupole doublets. These doublets use nonlinear focusing to reduce the amplitude of beam halo particles while leaving the beam core untouched. This "tail-folding" would permit larger collimation amplitudes, which in turn reduces the amount of beam power intercepted and impact on beam dynamics due to wakefields. In the interest of conservatism, the collimation system design described above does not take this tail folding into account in the selection of apertures and other parameters. The octupoles are supplied as a reserve measure in case the primary collimation system does not perform as expected and/or the beam halo is worse than anticipated.

For the higher-energy, advanced accelerator concepts, such non-linear collimation systems will be essential to consider to reduce the higher levels of halo particles impacting the collimation systems.

2.6 Final focus

The role of the final focus (FF) system is to demagnify the beam to the required size (≈ 639 nm (horz) and ≈ 5.7 nm (vert)) at the IP (in the case of ILC). The FF optics creates a large and almost parallel beam at the entrance to the final doublet (FD) of strong quadrupoles. Since particles of different energies have different focal points, even a relatively small energy spread of $\sim 0.1\%$ significantly dilutes the beam size, unless adequate corrections are applied. The design of the FF is thus mainly driven by the need to cancel the chromaticity of the FD. The ILC FF has local chromaticity correction [6] using sextupoles next to the final doublets. A bend upstream generates dispersion across the FD, which is required for the sextupoles to cancel the chromaticity. The dispersion at the IP is zero and the angular dispersion is about $\eta'_x = 0.009$ (small enough that it does not significantly increase the beam divergence). Half of the total horizontal chromaticity of the whole final focus is generated upstream of the bend in order for the sextupoles to simultaneously cancel the chromaticity and the second-order dispersion. The sextupoles also generate third-order geometric aberrations, where additional sextupoles placed upstream, and in proper phases with the FD sextupoles, partially cancel these.

Synchrotron radiation from the bending magnets causes emittance dilution, so it is important to maximize the bending radius, especially at higher energies. The FF includes sufficient bend magnets for 500 GeV Center-of-Mass energy (CM) and space for additional bend magnets which are necessary at energies above 500 GeV CM. With the reserved space filled with bends, the emittance dilution due to bends at 1 TeV CM is about a percent, and at 500 GeV CM, with only every fifth bend installed, about half of that. In addition to the final doublet and chromaticity correction optics, the final focus includes additional absorbers for the small number of halo particles which escape the collimation section; tail folding octupoles; crab cavities; and additional collimators for machine protection or synchrotron radiation masking of the detector. The specific design philosophy for the FF (the "local chromaticity correction" scheme) has many advantages over previous schemes, such as reduced system length and improved energy bandwidth [6]. Like the previous designs, this system is, however, operationally complex as it allows for some parameters to be further pushed, such as L^* increase (see later). The set of high-order magnets (sextupoles and above) required to cancel the FF chromaticity involves careful cancellation of various high order terms in the non-linear transport of the beam. This fine cancellation is disturbed by small placement and strength errors, in addition to other common manufacturing imperfections in the magnets. These equate to tolerances that are too tight to achieve in an "as-built" configuration. Instead, online tuning algorithms are designed to restore the aberration-cancellation of the FF magnet system. These include μm-level positional and rotational coordinated moves of multiple sextupole magnets in addition to magnetic field changes to sextupole, and higher-order magnets.

The degree of difficulty of this tuning procedure is governed by the magnitude of the FD chromaticity, given approximately by the ratio of L^* (drift distance between final FD magnet and IP) to β_y^* (vertical beta function at IP waist location). Typically, the L^* is required to be as large as possible to separate the FD from the detector. As luminosity needs to increase along with beam energy to compensate for the lowering of expected particle interaction cross-sections, this requires smaller β_y^* to avoid pushing the beam power too high. This in turn requires a FD with higher chromaticity and a correspondingly harder to tune FF system. The use of a plasma-focusing system in place of the FD would help greatly in this regard. Increasing levels of tuning difficulty due to higher FD chromaticity manifests in various ways: the length of time required to tune to design luminosity increases due to breakdown in orthogonality of the multiknobs constructed to perform the tuning; the final luminosity achieved is reduced due to imperfect tuning; the rate at which the luminosity degrades due to "random walk" of variables (e.g. ground motion, both natural and vibrational caused by accelerator components, magnetic power supply jitter and drift etc.) increases. These all lead to a restriction in the maximum available luminosity which is dependent on the FD chromaticity in a non-trivial way.

To experimentally demonstrate the plausibility of this newly designed FF scheme, a test facility at KEK, Japan (ATF2) was constructed in 2006. The design of ATF2 provides an energy-scaled test of the FF optics intended for ILC and successfully demonstrated correction of the FD chromaticity from the same levels as required at ILC [7]. A comprehensive description of the FF tuning procedure, simulations and experimental tests can be found in [8].

2.7 Energy bandwidth

The vertical beam size is dependent on the FF chromaticity due to the FD and the incoming energy spread of the beam. Chromaticity is defined as the energy dependent dilution of the IP beta function: $\xi = \frac{d\beta^*/d\beta^*}{\delta_E}$, which roughly scales as L^*/β^* [6], where β^* is the (vertical) IP beta function of
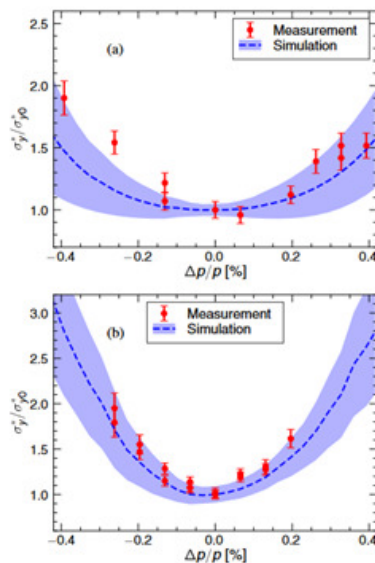
Figure 3. Energy bandwidth of ATF2 FF, simulated and measured, reproduced from: [9]. Top plot shows the bandwidth of the system tuned with the same FD chromaticity as ILC, lower plot shows tuning simular to CLIC with approximately 4 times the chromaticity.

the lattice at the interaction point, δ_E the rms relative energy spread of the beam and L^* is the distance from the center of the final quadrupole magnet to the IP. Although the FF optics are designed to remove the chromatic beam size growth as described above, higher-order chromatic and chromo-geometric aberrations arise in the lattice from higher-order contributions from the multipolar magnets and from lattice imperfections. See [9] for a fuller account. This chromatic dependence can be depicted as the energy bandwidth of the BDS optics, calculated by measuring the rms vertical beam size as a function of beam energy offset (either directly or theoretically using tracking simulations). The ATF2 test FF optics were designed with the same chromatic response function as ILC [7]. The energy bandwidth of these optics has been analytically calculated and directly measured [9], see figure 3. The simulated energy bandwidth includes treatments of known error sources and specifics of the beam size measurement. As shown, increasing the FD chromaticity (here by a factor of 4) reduces the energy bandwidth considerably.

As can be seen, the FF optics is extremely sensitive to off-energy particles, with requirements typically that the particles deviate $\ll 0.5\%$ in energy from design. The energy bandwidth further narrows as the focusing requirements become tighter in higher energy colliders, which also typically have acceleration mechanisms which generate higher energy spread beams than the current Linear Collider designs. The bandwidth can be broadened through the use of more high-order magnets at the expense of greatly tightening up (already tight) system tolerances. Again, the use of plasma focusing optics in place of a conventional FD here would help dramatically.

2.8 Feedback systems and collision stability

The greatest source of instability is from transverse jitter of the FD, where the parallel-to-point focusing of the beam means FD jitter at the ~ 1 *nm* level gives rise to substantial luminosity loss as

the beams are taken out of precise collision. Reliance on strong beam-focusing for smaller values of β^*, required at Multi-TeV colliders, further enhances this sensitivity due to the highly non-linear beam-beam dynamics (see later section of beamstrahlung). The long bunch trains of ILC affords a possibility of mitigating this luminosity loss through the use of an intra-train beam-based feedback. This detects the strong beam-beam deflections generated by these small transverse offsets simply by measuring the downstream beam trajectory on a stripline BPM monitor. Such a system can be utilized in either e+/e- or e-/e- collisions [10]. Additionally, an intra-bunch, high-bandwidth feedback based on the vertical collision angle is used to optimize the position and angle offsets of the collision. This helps correct for systematic bunch shape distortions due to short-range transverse wakefield effects in the main linac in the presence of finite beam orbit offsets.

Augmenting the fast bunch-by-bunch feedbacks are slower inter-train feedbacks operating at a few Hz, used to correct for long-term drifts. Finally, an additional high-bandwidth feedback is used at the entrance to the BDS to "straighten" the bunch train which can contain systematic distortions (non-linear time-dependent transverse offsets within the ms long bunch train) due to long-range wakefield kicks in the linac.

Many advanced acceleration technologies are not compatible with operations with long bunch trains, with ~ ns scale temporal bunch separations like ILC. Here, the final focusing elements must be dynamically stabilized to very fine $< nm$ precision to ensure stable bunch conditions. The CLIC collaboration has demonstrated [11] nm-level stability precision, where their shorter bunch trains and smaller IP spot sizes demands this. At higher energies, and with tighter focusing at the IP, this challenge becomes more pronounced. Additionally, reliance on plasma focusing elements generates an additional source of jitter at this sensitive location.

2.9   Machine detector interface, extraction systems and beam dumps

There are many further issues to consider in the interface of the BDS with the physics detector(s) and with the magnetic system used to extract the beam after collision and safely transport it to a (multi-MW) dump. The potential design of a future multi-TeV collider is not yet mature enough to understand yet how to extend the current designs, and work has not yet started on such studies. We list here a few areas which will require attention in future design efforts.

2.9.1   Crab cavities

Existing LC designs utilize a crossing angle at the IP to assist in the design of the beam extraction system which has to deal with a highly disruptive, high energy spread beam post-collision. The inclusion of a crossing angle also avoids deleterious effects due to parasitic interactions between incoming and outgoing beams in a tightly packed bunch train.

Typically, the advanced collider concepts considered here do not consider trains of bunches, rather a higher repetition rate, CW collision. In this case, parasitic interactions are not an issue. However, operation with higher beamstrahlung increases the energy spread of the post-collision beam which may necessitate a crossing angle to be able to cleanly extract.

Applying a (horizontal) crossing angle to the beam causes a loss in luminosity which scales as $C_\theta = \theta_c \sigma_z / \sigma_x$, where θ_c is the crossing angle in radians and $\sigma_{x,z}$ is the rms horizontal beam size and bunch length at the IP. A value of $C_\theta = 1$ corresponds to a 10% luminosity loss.

The luminsoity loss due to the crossing angle is mitigated in ILC and CLIC designs through the use of crab cavities which use a deflecting rf field to give the bunches a z-dependent offset so that they collide head-on. The crab cavity for the ($E_{\text{cm}} = 1$ TeV) ILC design uses two 9-cell L-band cryogenic cavities (each in a 3 m long cryostat) to provide a 5 MV/m peak deflection for the 14 mrad crossing angle. The required rf voltage scales linearly with the beam energy, crossing angle and rf wavelength.

The most critical tolerance on the crab cavity system is given by the relative phase between cavities on each side of the collision point. Such a phase difference causes an x offset between the colliding beams. To limit the luminosity degradation to 2%, the bunch separation must be $< 0.3\sigma_x$ rms, which in turn requires $\Delta\theta_{\text{rf}} < 2\pi\frac{0.6\sigma_x}{\Theta_c\lambda_{\text{rf}}}$ (see section 4.6 of [12]), where Θ_c is the crossing angle and λ_{rf} the rf wavelength.

2.9.2 Effects of the detector solenoid

The field of the detector solenoid produces beam coupling and, when including a crossing angle, it also generates additional dispersion and vertical trajectory through the IP region. This latter point also resulting in additional IP beam size growth from synchrotron radiation. In an ideal case, symmetry in the path of the incoming beams (for the case of electrons and positrons) is preserved and coupling effects and offsets cancel. If the final doublet magnets, for instance, are required to be within the solenoid field (as for ILC) then this symmetry is broken. A "detector integrated dipole" can be integrated into the detector solenoid, producing a sine-like transverse field through the detector. This allows for compensation of the angle at the IP and minimization of the vertical orbit (and hence reduction in the synchrotron radiation induced emittance dilution). However, for ILC, it was determined that a negative polarity integrated dipole field be used instead (a so-called "anti-DID"). The anti-DID field being optimized to guide the low energy electron-positron pairs generated in the beam-beam collision into the extraction beam aperture and reduce backgrounds. Here, this was considered a more important design consideration rather than the small luminosity impact of the dipole field itself when considering the full physics program. Several scaling relations treating these various effects can be found in [12] and references therein.

3 ILC vs. CLIC

The CLIC design philosophy is much more aggressive than ILC, as has been required for considered operations at 3 TeV. For example, the primary collimation system is designed to handle 100X less halo (fractionally) and the pre-alignment tolerances need to be 30X better than ILC. Despite focusing the beam tighter than ILC, the FF optics has a shorter length footprint than ILC, with a larger L^*, resulting in much higher chromaticity and requiring a much more complex correction system. Hence, even at 3X the design energy, the footprint of the CLIC BDS is similar to ILC (see figure 4). This comparison well demonstrates the trade-offs available between performance, cost, and risk.

An attempt has been underway for several years at ATF2 to demonstrate the ability to tune the FF with levels of chromaticity similar to CLIC (by reducing β_y^*), which involves the addition of octupole magnets to the machine. It should be noted at the time of writing, that the achieved beam size in this configuration is still larger than that achieved for the ILC configuration [13] demonstrating the increased level of difficulty in tuning this presents.
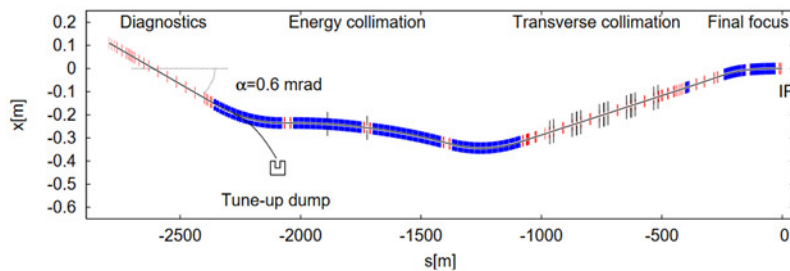
Figure 4. Schematic showing layout of CLIC BDS [11].

4 Energy scaling of BDS length

We attempt here to examine how the overall length of the BDS changes with design beam energy. We use the baseline design of the ILC or CLIC BDS as a reference (see table 1). We examine the BDS in 3 different sections: the final focus system (FFS), the bending systems (various diagnostics and energy collimation chicanes), and the other systems (transport, matching, betatron collimation and other beam diagnostics sections).

Table 1. Path length of ILC and CLIC BDS.

	ILC (E_{cm} = 1 TeV)	CLIC (E_{cm} = 3 TeV)
FFS	826 m	446 m
Bending sections	562 m	1250 m
Other	866 m	1054 m
Total	2254 m	2750 m

4.1 Bending sections

Normalized emittance degradation in the bending systems due to incoherent synchroton radiation is generated in the bending plane according to: $\Delta\epsilon_N \approx (4 \times 10^{-8}\,\mathrm{m^2\,GeV^{-6}})E^6 \sum_i \frac{L_i}{|\rho_i|^3}\mathcal{H}_i$ [14], where ρ is the bending radius and $\mathcal{H}$ is a function of the lattice parameters through the section. The subscript i indicates a summation over all bending elements in the lattice. Making the assumption that these sections are dominated by the bending magnets and that the target lattice parameters and required target dispersion remain the same, we thus make the assumption that the length in these sections scale according to the need to increase the bend radius: $L \sim E^2$.

4.2 Matching / transport / diagnostics / collimation sections

The MPS and betatron collimation systems, coupling correction and emittance measurement systems, extraction systems, and matching optics between the various BDS subsystems are dominated by the quadrupole focusing magnets required to perform the desired betatron manipulations. We use here the energy scaling of a FODO system to represent the scaling behavior of this ensemble of systems. Using the fact that the BDS length for ILC has been optimized, including for overall length considerations, we scale the lattice length from the designed energy assuming a scaling of the

quadrupole focusing length parameter with energy. Using the usual transport matrix approximation for a FODO cell with thin-lens quadrupole elements, it can be shown that the phase-advance is related to the length of the cell as: $sin(\theta/2) = L_{\text{cell}}/(4f)$. Using a fixed phase advanced as a proxy to maintaining the functionality of the various subsystems, the length of these systems is scaled simply as $L \sim E$.

4.3 Final focus system

Scaling of the local-chromaticity correction style of final focus used in ILC is discussed in the original design paper for this style of optics by Raimondi/Seryi [6]. For fixed emittance, the FFS length scales as $E^{7/10}$. Again, the main constraint here is the emittance growth in the bending systems of the FFS. This does, however, make assumptions about the scalability of field gradients in the FFS quadrupoles, especially the final doublet, which may not be reasonable. Another assumption is that the IP beta functions and chromaticities remain constant (equivalent to holding L^* and the length of the final doublet quadrupoles constant). This is also not reasonable due to limitations in possible quadrupole strengths and the need to achieve higher luminosities at higher energies. Also, there is freedom in the design of this style of FFS to trade-off length with tolerances (which relates to risk of operation through increased difficulty in tuning).

Given the complexities involved in the FFS, it is not really feasible to pin down an analytic scaling law that takes into account the changing needs of the system design as one moves to higher energies, or properly take into account the changing complexities of the tuning system, without performing extensive design evaluations at each energy. For the sake of this analysis, we nevertheless use the only option of utilizing the $E^{7/10}$ scaling motivated by [6].

4.4 Overall scaling

As shown in figure 5, whilst the final focus system itself looks to be scalable to the $\sim 10\,\text{TeV}$ energy scale within a reasonable length footprint (few km) (with the many caveats stated earlier), the various other systems which comprise the BDS do not scale so favorably. Note, however, the discrepancy between the scaled length of ILC at 3 TeV and the custom design length of CLIC at that energy. This difference comes from the CLIC design being significantly more aggressive than ILC: less risk-averse and more optimistic about background conditions and ability to handle tolerances which are orders of magnitude tighter than ILC.

5 Extensions to existing BDS designs: selected topics

5.1 Beam aspect ratio

From the collider point of view, beams with a large aspect ratio (i.e. $\sigma_x/\sigma_y \gg 1$), or flat beams, have the advantage of reduced beamstrahlung effect at the interaction point, without sacrificing the peak luminosity. In a plasma accelerator, it is relatively unclear if flat beams will perform as well as round beams due to the asymmetry in beam loading, which could potentially lead to deterioration in beam quality. This is especially relevant for positrons, as no reliable acceleration regime has yet been identified. Since flat beams are considered to be supreme in reaching high peak luminosities in colliders, the effect of beam loading in accelerators for flat beams will be studied in parallel to achieve synergy.
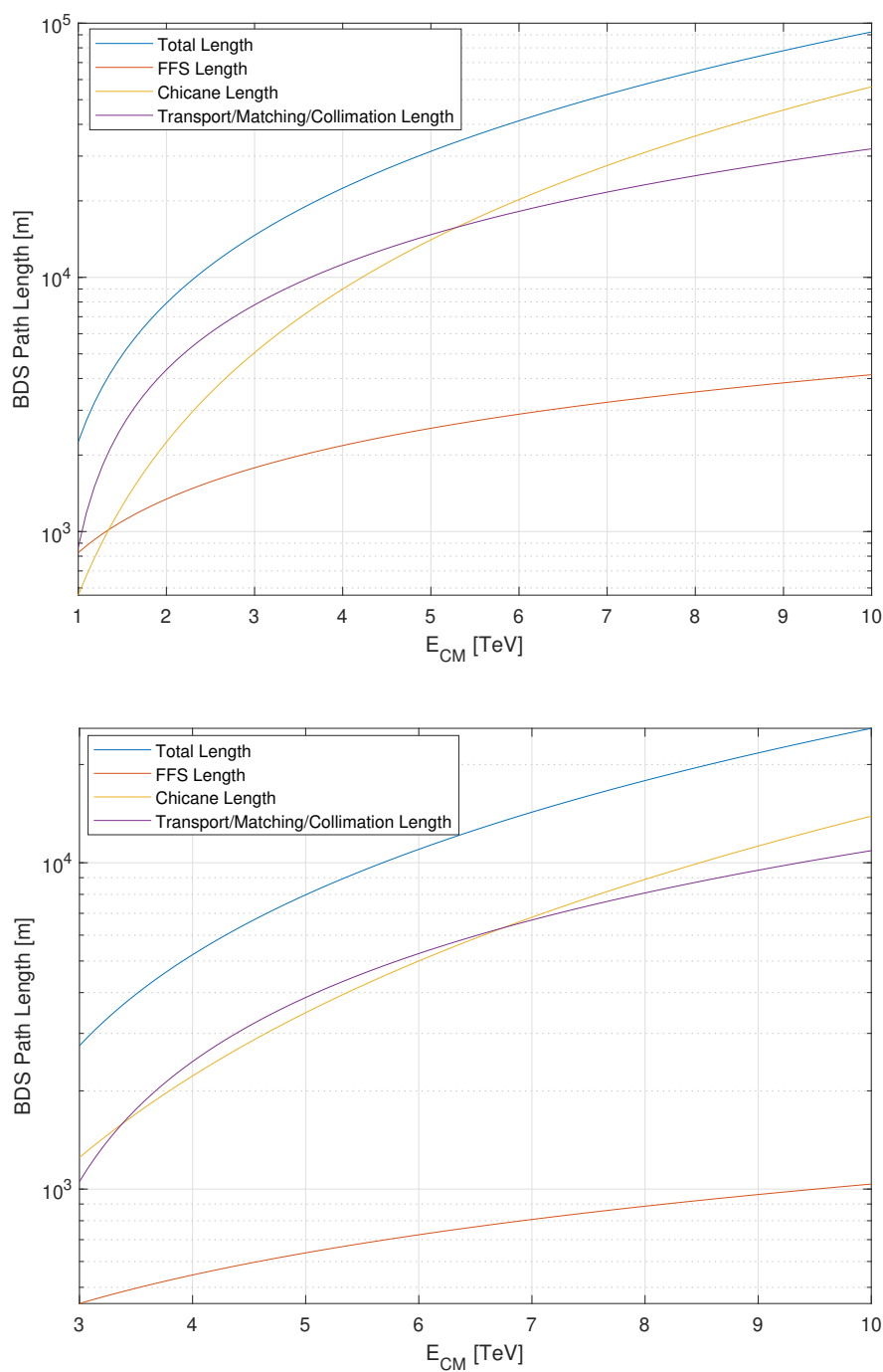
Figure 5. Path length of ILC (top) and CLIC (bottom) BDS as a function of collision energy using the scaling laws outlined in section 4. "Chicane Length" refers to the sum of all bending sections.
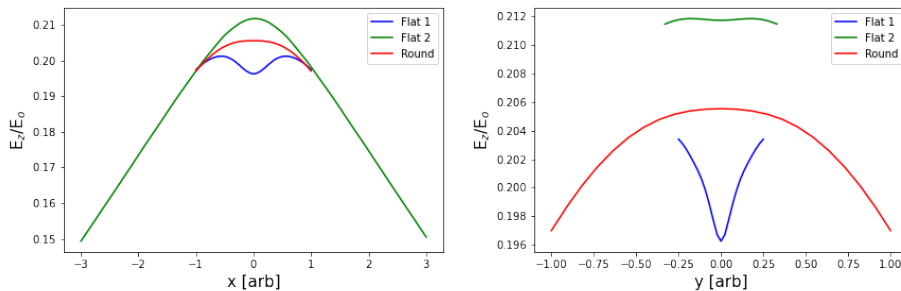
Figure 6. Central slice of the accelerating field (or overall energy profile) at 3σ level for flat and round beams in x (left) and y (right) direction. The x-axis shows the relative sizes of the beams. The two flat beams are defined, relative to the round beam — Flat 1: $\sigma_{x,\text{flat}} = \sigma_{x,\text{round}}$, $\sigma_{y,\text{flat}} = \frac{1}{4}\sigma_{y,\text{round}}$ where $\sigma_{x,y}$ are the RMS sizes in the respective dimensions. Flat 2: $\sigma_{x,\text{flat}} = 3\sigma_{x,\text{round}}$, $\sigma_{y,\text{flat}} = \frac{1}{3}\sigma_{y,\text{round}}$. The beam charges are kept constant.

A preliminary study on positron beam loading in a moderately non-linear regime for a round/flat beam is shown in figure 6. The results demonstrate that for a flat beam with $\sigma_{x,\text{flat}} = \sigma_{x,\text{round}}$ and $\sigma_{x,\text{flat}}/\sigma_{y,\text{flat}} = n_{\text{flat}}/n_{\text{round}}$, the uncorrelated energy spread (or the slice energy spread), can be preserved to approximately the same level as the round beam. The uncorrelated energy spread is defined as $\delta = \frac{1}{\langle E_z \rangle}\left[\frac{1}{N_b}\int \left(E_z(x,y,\xi) - \langle E_z \rangle (\xi)\right)^2 n_b dx dy d\xi\right]$ [15], where $\langle E_z \rangle$ is the average longitudinal electric field acting on the beam, N_b the total beam charge and n_b the beam density. The increase in δ is within 10% in this case. For a flat beam with $\sigma_{x,\text{flat}}\sigma_{y,\text{flat}} = \sigma_{x,\text{round}}\sigma_{y,\text{round}}$, the underloading in the x direction shown in the figure deteriorates greatly δ with an increase of a few factors. A more complete study on overall beam quality and energy efficiency will be performed. From the preliminary study, it is apparent that the beam density, in addition to the aspect ratio, could set an important limit on beam quality. This could in turn affect the possible flatness of the beam at IP. To be able to accommodate eventual positron acceleration schemes, both round and flat beams will be studied. Therefore, future work on asymmetrical beam collisions (i.e. colliding a flat electron beam with a round positron beam) is planned.

On the other hand, the quantitative effects on luminosity with varying aspect ratios need to be studied in detail and complement the flat/round beam study in a plasma accelerator. Previous studies parameterised the effect of aspect ratio in terms of the effective transverse sizes [16]. A preliminary comparison in luminosity performance for flat and round beams is made and the results are shown in figure 7. While round beams lead to higher total luminosity due to larger enhancement from mutual pinching between the two dimensions, the spread in the colliding beam energy spectrum due to beamstrahlung results in a much reduced peak luminosity compared to flat beams. The study aims to synergize the collider and accelerator sections for the beam in terms of the aspect ratio and find feasible parameter ranges that would satisfy both the luminosity and beam quality requirements.

The specific case of round-beams at the IP is interesting to consider from the perspective of the FFS. It has been observed both experimentally (at ATF2) and through simulations for ATF2 and ILC, that tuning difficulties become enhanced as the IP horizontal beta function is reduced [8]. Further, for equal beta functions at the IP, a final triplet of quadrupole magnets in place of the FD is appropriate due to reduced chromaticity for this style of optics. A small (< 1 mm) beta focusing system for a triplet based optics has not yet been demonstrated. It is possible to follow the design philosophy
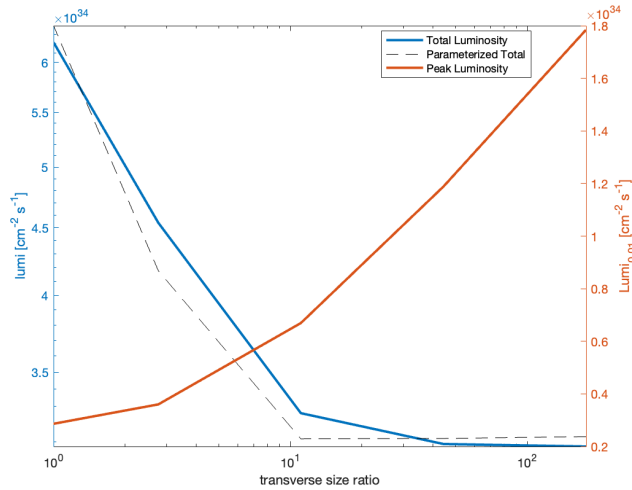
Figure 7. The simulated total and peak (i.e. the luminosity corresponding to particles colliding at $\sqrt{s} > 0.99\sqrt{s_o}$) luminosity over a range of aspect ratios ($\sigma_x\sigma_y$=constant). $\sqrt{s}$ is the center-of-mass energy of the colliding beams with beamstrahlung effect taken into account, and $\sqrt{s_o}$ is the nominal or the design center-of-mass energy of the collider. The parameterised total luminosity is calculated using the parameterization of the effective transverse sizes given in [16].
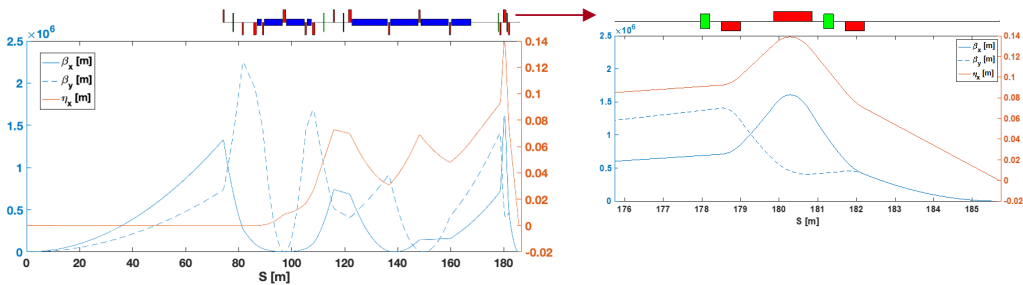

Figure 8. Final focus system optics design for an $E_{cm} = 250\,GeV$ collider with round-beam IP configuration ($\beta_x^* = \beta_y^*$).

outlined in [17], as shown in figure 8. Further work is required to understand the tunability and associated tolerances of such a design.

5.2 Plasma lenses

5.2.1 Passive plasma lenses

Plasma lenses can focus electron beams with strengths several orders of magnitude stronger than quadrupole magnets [18–20]. In passive plasma lenses, the transverse focusing force in the underdense, nonlinear blowout plasma wake regime is due to the presence of the stationary plasma ions. If the transverse density profile of this ion column is uniform, then the focusing force experienced by the electrons in a relativistic beam is both axisymmetric and linear. These properties lead to an aberration-free focus of the beam that can achieve unprecedented small beam spots. The first order beam dynamics have been described in ref. [18].
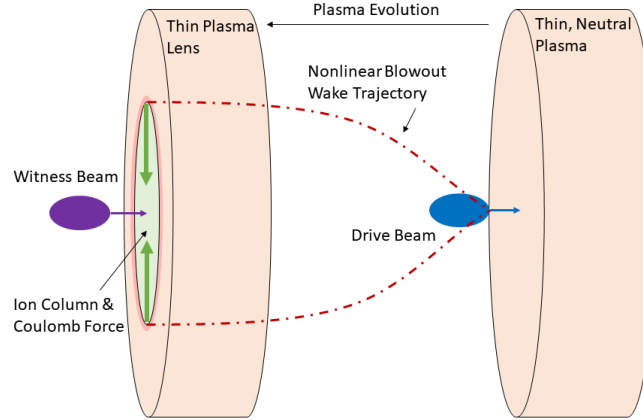
Figure 9. Illustration of the underdense, passive plasma lens. A dense drive beam drives a nonlinear blowout wake in an underdense neutral plasma, and a subsequent witness beam is focused by the Coulomb attraction of the stationary ions. The force is axisymmetric and linear so long as the witness beam is fully within the blowout wake and the plasma density is uniform.

The underdense plasma lens (UPL) operates in a two-bunch configuration where a "driver" electron bunch drives the nonlinear wake and a second, "witness" electron bunch is subsequently focused in the nonlinear blowout wake (figure 9). It may also be possible to operate in a single-bunch configuration where the head of the electron bunch drives the nonlinear wake and the bulk of the electron bunch is focused. In this regime, the linear focusing force from the ions results in a focal length given by the focusing strength

$$f \equiv \frac{1}{KL} = \frac{1}{2\pi r_e} \frac{\gamma_b}{n_p L}.$$ (5.1)

Here, K is the focusing strength, L is the lens's longitudinal thickness, r_e is the classical electron radius, γ_b is the Lorentz factor of the electron beam, and n_p is the plasma density of the lens. A UPL with a plasma density of $n_p = 1 \times 10^{17}\,\text{cm}^{-3}$ can have a focusing strength $K = 88400\,\text{m}^{-2}$ and focal length $f = 3.3\,\text{cm}$. For comparison, a conventional quadrupole with field gradient $G = 1\,\text{T/m}$ would have $K = 0.3\,\text{m}^{-2}$ and focal length $f = 1000\,\text{cm}$ and a permanent magnetic quadrupole with $G = 500\,\text{T/m}$ can expect $K = 150\,\text{m}^{-2}$ and focal length $f = 81\,\text{cm}$.

The UPL can be generated by laser ionization of gas, e.g. by focusing a femtosecond laser pulse into a gas jet. To minimize the footprint, the laser pulse can propagate transverse to the electron beam axis, reducing the required space along the beam line to millimeters. The longitudinal density profile of the plasma lens is then given by the laser parameters and focusing optics for gas ionization. Something as simple as a Gaussian focus from a spherical lens with a variable offset from the laser focus to the beamline can give a plasma lens thickness 10's–100's µm.

There has been discussion about the potential use of a plasma lens for the final focusing element of a collider for decades [19, 20]. The strong, linear, axisymmetric focusing of the UPL in combination with its ultra-compactness and "self-aligning" characteristics may show it to be a viable candidate, although further study is still required. It should be noted that the functionality of the UPL described above applies only to negatively charged relativistic leptons. Relativistic positrons would experience a linear *defocusing* force in this scheme. It may be possible to achieve similarly
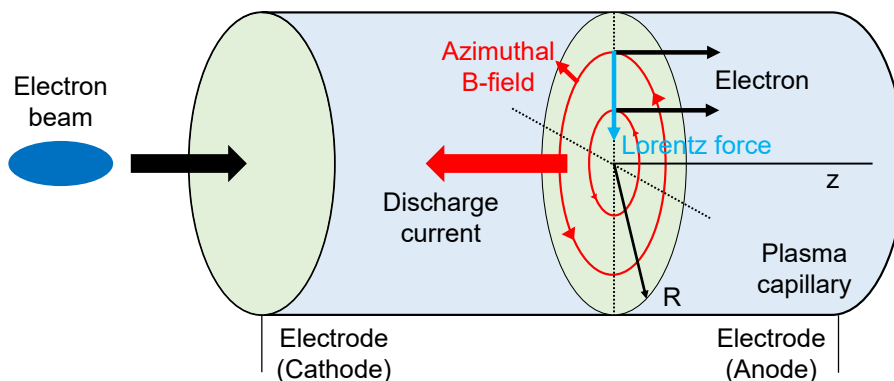
Figure 10. Schematic illustration of an active plasma lens. From [22].

strong focusing with the UPL if the positrons are sent through the lens in a different phase of the nonlinear wake, where the plasma electrons have returned on-axis or by using a plasma column of finite radius as in [21], but this is speculative. Another important consideration is the scattering of the beam off of the plasma ions, which may produce both an increase in the beam emittance and a forward-directed shower of secondary particles. The former could result in a reduced luminosity and the latter could result in an increased background for the particle detectors.

5.2.2 Active plasma lenses

Active plasma lenses (APL), illustrated in figure 10, are magnetic focusing devices that work by passing a strong current though a plasma, on the same axis as the beam. This creates an azimuthal uniform magnetic field inside the plasma that produces axisymmetric focusing, unlike a quadrupole that focuses in one plane and defocuses in the other. The field inside is given by the current distribution in the lens, and in the ideal case with a uniform current distribution and with a circular aperture with radius R, we have the magnetic field as a function of radial position r

$$B_\phi(r) = \frac{\mu_0 I}{2\pi} \frac{r}{R^2} = g_{\text{APL}} r \,. \tag{5.2}$$

Here I is the total current in the lens, and g_{APL} the magnetic gradient. Current APLs typically use a gas-filled capillary with electrodes on either side, powered by a high voltage source that drives a large current through the lens. They have lengths of a few mm to many cm and aperture diameters a few hundred microns to mm-scale.

Naturally, the linearity of the focusing field is critical for preserving the beam emittance. When used with lighter gases such as hydrogen or helium, a temperature gradient between the center of the lens and the wall can cause a nonuniformity in the conductivity and thus the current density, leading to a nonlinear field and emittance increase [23–26]. Nonlinearity in the field can also arise due to the z-pinch effect [27], in which the drive current is self-focused towards the axis [28–30], reducing the radius over which the lens is linear. This could present a limitation of the ultimate field strength in an active plasma lens.

On the other hand, it has been demonstrated that with a heavy gas like argon, APLs can have a uniform current distribution and thus a linearly increasing magnetic field, preserving the

emittance [26, 31]. The linearity of the field has been demonstrated up to a gradient of 3.6 kT/m in a capillary with diameter of 500 μm [32].

While the effective focusing strength of an APL is an order of magnitude higher than standard quadrupoles, it is 2–3 orders of magnitude weaker than the UPL. However, APLs do not require a beam driver, making them compact and simple to operate [33]. They also can be easily configured to focus electrons or positrons; one only need switch the sign of the current (i.e. put the high voltage electrode on either the upstream or downstream side of the APL).

A challenge in using APLs in focusing of high brightness, high intensity beams arises from the impact of self driven wakefields. In other words, passive plasma lensing will also occur in an APL if the beam density is sufficiently high. These generated fields are a complex function of both APL and beam parameters and generally are neither linear or easily tunable [34]. The impact of self driven wakefields can be mitigated to an extent by using shorter lenses with higher gradients, and shortening the plasma density ramps is one way of reducing this effect [22]. Additionally, self driven wakefields have a strong dependence on the bunch length, with shorter bunches being more favorable. This scaling is naturally conducive to emerging interest in the use of attosecond-scale bunches for future high luminosity colliders [35].

5.3 Trade-offs between bunch charge and repetition rate

When considering the range of parameters in the collider design, it is important to consider the non-linear effects present in the beam-beam interaction. This is demonstrated here in a consideration of the bunch charge and machine repetition rate for a structure wake-field accelerator (SWFA) collider design.

A numerical simulation has been carried out at the interaction point to investigate possible trade-offs between the charge of individual bunches and the repetition rate of a linear collider. The luminosity calculation was performed using the Guinea-PIG [36] code, taking into account the pinch effect, beamstrahlung, pair creation. The results are presented in figure 11.
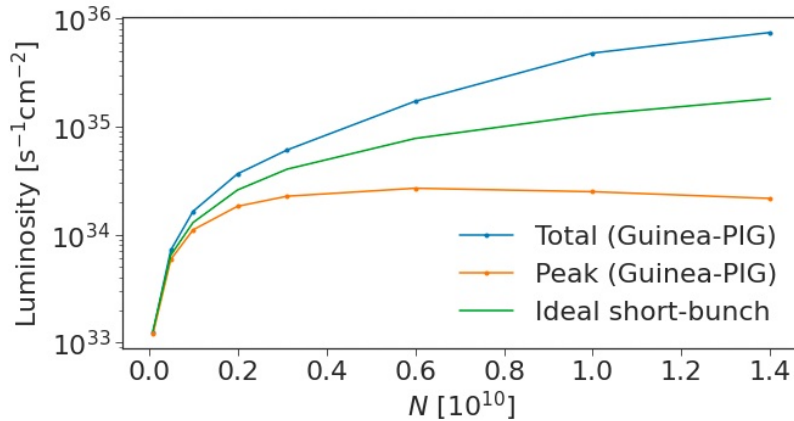
Figure 11. Calculated luminosity as a function of bunch charge. Total charge per second is kept constant by adjusting the repetition rate accordingly, i.e., $f_{rep}n_b N$ = const.

In this simulation, the number of electrons (positrons) N in one bunch is varied in the range from 1.0×10^8 to 1.4×10^{10}. However, the total beam power is kept constant. This is achieved by keeping the total delivered charge per second constant (i.e., $f_{rep}n_b N$ = const) by changing

the repetition rate f_{rep} accordingly. The number of bunches per train $n_b = 208$ is kept the same. The normalized transverse beam emittances and the bunch length were $\epsilon_x = 0.66 \times 10^{-6}$ m rad, $\epsilon_y = 0.02 \times 10^{-6}$ m rad, and $\sigma_z = 44.0\,\mu$m, respectively, at all values of N. The longitudinal density distribution was normal. The transverse beta functions at the interaction point were $\beta_x = 7.1$ mm and $\beta_y = 0.15$ mm, the center of mass energy was $s_o = 3.0$ TeV.

Figure 11 presents the total and the peak luminosity (blue and orange lines, respectively) calculated using Guinea-PIG. The peak luminosity is the luminosity calculated for the particles colliding with the energies above 99 % of initial energy, i.e., $\sqrt{s} > 0.99\sqrt{s_o}$. The green line corresponds to the ideal short-bunch approximation for the luminosity [37]

$$\mathcal{L}_{00} = \frac{f_{rep}n_b N^2}{4\pi\sigma_x\sigma_y},\tag{5.3}$$

which does not account for luminosity enhancement, beamstrahlung, etc.

Figure 11 illustrates that the total luminosity and the ideal short-bunch luminosity monotonically increase with the number of particles in one bunch N, as expected. However, the peak luminosity has a maximum at a certain N. Indeed, after some N, the increase due to the N^2 dependence in eq. (5.3) is overpowered by the reduction due to beamstrahlung. This observation is important if the objective is to achieve higher peak luminosity. In the present SWFA design, $N = 3.12 \times 10^9$ and $f_{rep} = 100$ Hz. Figure 11 shows that the maximum peak luminosity is achieved at $N = 6 \times 10^{10}$ and $f_{rep} \approx 50$ Hz.

The presented simulation did not account for the likely change in bunch dimensions due to the change in bunch charge. However, if it was taken into account, the maximum in the peak luminosity in figure 11 would perhaps be even more pronounced: bunch dimensions would grow with bunch charge and the peak luminosity would descend faster on the right-hand slope of the curve. Also, the bunches were assumed to be Gaussian, which is not exactly true due to the Oide effect [38].
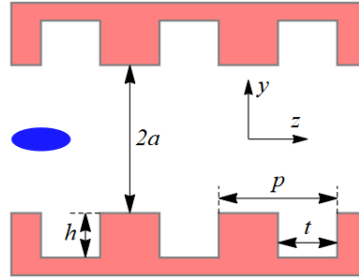
5.4 De-chirper

Advanced multi-TeV acceleration concepts may require the use of instability mitigation techniques, including generation of strong head-tail energy chirps applied to the accelerating beam. One downside of such a scheme will be having to accept bunches with higher energy spread into the BDS than considered for existing linear collider designs. As discussed earlier, this leads to a severe degradation in luminosity or increase in tuning complexity when operating the BDS. Once the acceleration of the bunch is complete, one mitigation scheme might be the use of a "de-chirping" device to remove the head-tail energy chirp and reduce the energy spread of the beam presented to the BDS.

An example of using a de-chirper device to remove the energy chirp from a short bunch has been studied for the LCLS accelerator [39], for which a schemtic is shown in figure 12. The corruogated structure sits close to the beam inside the vacuum chamber and generates a strong longitudinal wake. The idea is to use this passive device to remove residual energy chirp in the beam before it enters the FEL undulator for lasing. Here, we could consider a similar structure at the entrance to the BDS to perform a similar function.

The average beam energy loss for such a device, for a pencil-beam, is [39]

$$(E_w)_{av} = \frac{\pi}{32a^2}Z_0 cqQL\sec^2\frac{\pi y}{2a},\tag{5.4}$$

where Q is the bunch charge, L the dechirper length, and other parameters as depicted in figure 12.

Figure 12. Geometry of a horizontal dechirper from [39]. A rectangular coordinate system is centered on the symmetry axis of the chamber. The blue ellipse represents an electron beam propagating along the z axis.

For LCLS, a dechirper structure of length 2 m and half aperture 0.7 mm, bunch charge 150 pC, bunch length 30 μm was calculated to generate a wake-induced energy loss of 6.8 MeV (with a 6.6 GeV energy electron beam at that stage of the accelerator). Using these figures as a guide, it is clear that an effective dechirping device for a multi-TeV collider will be quite formidable. With a dechirping requirement of multi-% energy spread, such a device based on this technology would need to be many 100's m in length with ≪ mm aperture. Alignment and control of transverse wakefield kicks will be a major consideration.

6 Physical limitations and effects on beam spot size

6.1 Oide effect

In 1988, Oide described the effect of hard synchrotron photon emissions in a strongly focusing quadrupole magnet on the emittance of a beam [40]. This emittance growth results in a minimum achievable final spot size, referred to as the Oide limit. This is not a hard limit, as the magnitude of the effect due to hard synchrotron radiation depends on the strength and length of the focusing optic, as well as the incoming beam parameters. In the Oide model, the minimum achievable final spot size is given by:

$$\sigma_y^* = \left(\frac{7}{5}\right)^{1/2} \left[\frac{275}{3\sqrt{6\pi}} r_e \lambdabar_e F(\sqrt{K}L, \sqrt{K}l^*)\right]^{1/7} (\epsilon_{Ny})^{5/7} \tag{6.1}$$

with classical electron radius r_e, Compton wavelength $\lambdabar_e$, normalized emittance ϵ_N, focusing gradient K, lens thickness L, distance from the focus to the len's front end l^*, and where $F(\sqrt{K}L, \sqrt{K}l^*)$ is a dimensionless function that generally increases with focusing strength of the focusing optic and decreases with the thickness of the focusing optic.

On one end of the spectrum, a very thin and dense plasma lens operating in the underdense regime and focusing a large electron beam would produce a significant amount of hard synchrotron radiation and the Oide limit would be quite large. At the other end of the spectrum, the Oide limit could be completely suppressed if the incoming beam is capable of being adiabatically focused by slowly increasing the plasma density such that the beta function decreases linearly [41]. True adiabatic focusing from a plasma source could be difficult to achieve in practice, so future exploration into plasma-based final focusing systems will need to achieve a balance with lowering the Oide limit and generating a reasonable plasma source.

6.2 Beamstrahlung

Beamstrahlung, radiation emitted during the beam-beam interaction, can limit the charge per bunch at the IP. The beam-beam interaction is characterized by the Lorentz-invariant Beamstrahlung parameter [12], defined as the mean field strength in the beam rest frame $\gamma\langle E + B\rangle$ in units of the Schwinger critical field $E_c = m^2 c^3 / e\hbar$. For a Gaussian beam, the average beamstrahlung parameter is

$$\Upsilon \approx \frac{5r_e^2}{6\alpha} \frac{\gamma}{\sigma_z} \frac{N}{(\sigma_x + \sigma_y)}, \tag{6.2}$$

where α is the fine structure constant. For a given luminosity

$$\mathcal{L} = \frac{fN^2}{4\pi\sigma_x\sigma_x} = \frac{P_b}{4\pi E_b} \frac{N}{\sigma_x\sigma_y}, \tag{6.3}$$

fixed beam energy E_b and beam power P_b, the beamstrahlung parameter eq. (6.2) is reduced by using flat beams, i.e., $\sigma_x/\sigma_y \gg 1$. Beamstrahlung results in the emission of photons, unwanted background in the detector, and an increase in the effective beam energy spread owing to the energy loss. The number of photons emitted per lepton and the average relative energy spread induced by the beam-beam interaction in terms of the beamstrahlung parameter may be expressed [12] as $n_\gamma \simeq 2.54(\alpha^2\sigma_z/r_e\gamma)\Upsilon(1 + \Upsilon^{2/3})^{-1/2}$ and $\delta_\gamma \simeq 1.24(\alpha^2\sigma_z/r_e\gamma)\Upsilon^2[1 + (3\Upsilon/2)^{2/3}]^{-2}$, respectively.

Plasma and other advanced accelerator concepts propose to operate with ultrashort bunches. For example, plasma accelerators naturally produce beams with lengths that are a fraction of the plasma wavelength, $\sigma_z < \lambda_p$ (with, e.g., $\lambda_p \sim 100\,\mu m$ for plasma densities $n \sim 10^{17}\,cm^{-3}$). While conventional linear collider designs typically operate in the classical limit $\Upsilon \ll 1$, next-generation linear colliders using advanced accelerator technology with $\sqrt{s} > 1\,TeV$ will operate in the quantum beamstrahlung regime $\Upsilon \gg 1$, owing to the high beam energy and short bunch lengths. In this limit, $n_\gamma \propto \sigma_z\Upsilon^{2/3}$ and $\delta_\gamma \propto \sigma_z\Upsilon^{2/3}$. Hence, assuming a fixed luminosity $\mathcal{L}$, center of mass energy $\sqrt{s}$, and fixed beam transverse sizes at the IP σ_x and σ_y, the number of photons and induced energy spread scale as $n_\gamma \propto N^{2/3}\sigma_z^{1/3}$ and $\delta_\gamma \propto N^{2/3}\sigma_z^{1/3}$. On the other hand, for a fixed $\mathcal{L}$, P_b, $\sqrt{s}$ and transverse size ratio σ_x/σ_y, the number of photons and induced energy spread scale as $n_\gamma \propto (\sigma_z N)^{1/3}$ and $\delta_\gamma \propto (\sigma_z N)^{1/3}$. Shorter beam lengths will reduce the beamstrahlung degrading effects at the IP. Hence using advanced accelerator technology should allow one to operate at higher charge per bunch, reducing the power requirements to reach a target luminosity.

The beamstrahlung reduction enabled by short beams may allow one to consider operation with round beams, i.e., having symmetric transverse emittances. However, flat beams provide further beamstrahlung reduction and power savings. Assuming a minimum achievable 4D transverse emittance, partitioning the beam transverse phase space to achieve an asymmetric beam at the IP with $\sigma_x/\sigma_y = R$ can achieve the power savings: $\mathcal{L}/P_b \propto (R^{1/2} + R^{-1/2})\sigma_z^{-1/2}$, if limited by beamstrahlung.

Beamstrahlung also generates a source of background for the detectors through the production of coherent and incoherent electron-positron pairs which can be deflected to high angles in the strong colliding beam fields. Desire to keep beamstrahlung radiation small for the reasons stated above will also help mitigate such backgrounds, but careful analysis of these backgrounds is required to design detector shielding. Of specific concern for these high energy colliders will be high-order

QED processes which may become pertinent as the collision parameters move well into the quantum regime. All such processes may not yet have been incorporated into existing LC simulation software and special attention should be applied here.

7 Conclusion

When moving to high, multi-TeV, energies using advanced accelerator concepts, the BDS becomes a dominant subsystem due to the required length and the complexity in focusing, characterising and correcting of the beam at such high energies. So far, the focus in advanced collider concepts (correctly) has been on the acceleration technology itself. As we try to outline here however, the BDS presents many severe challenges and deserves a closer look moving forwards towards a final design.

A particularly severe aspect of moving to a multi-TeV collider is the scaling to many km of length due to the expensive length scaling of bending sections with energy. We simply considered here the required extensions to the BDS design based around the needs of a detector similar to the low-background, high collision purity of current electron-positron collider detectors. Should the physics case of this new multi-TeV scale of collider permit more aggressive detector designs, such extreme measures as elimination of the collimation system may be possible which would help in this aspect as the FFS itself may be kept to single-digits km in length for a 10 TeV collider for instance.

References

[1] ILC collaboration, *The International Linear Collider Technical Design Report*, V.3.11 (2013).

[2] J.T. Seeman, *The stanford linear collider*, Tech. Rep., SLAC-PUB-5494 (1991).

[3] CLIC collaboration, *The Compact Linear Collider (CLIC) — Project Implementation Plan*, CERN Yellow Reports, CERN (2018), 10.23731/CYRM-2018-004.

[4] M.D. Woodley and P.E. Emma, *Measurement and correction of cross plane coupling in transport lines*, *eConf* **C 000821** (2000) MOC19 [physics/0008194].

[5] P. Tenenbaum, *Collimator wakefield calculations for the ILC-TRC report*, Tech. Rep., SLAC-TN-03-038 (2002).

[6] P. Raimondi and A. Seryi, *A Novel final focus design for future linear colliders*, *Phys. Rev. Lett.* **86** (2001) 3779.

[7] ATF2 collaboration, *Experimental Validation of a Novel Compact Focusing Scheme for Future Energy-Frontier Linear Lepton Colliders*, *Phys. Rev. Lett.* **112** (2014) 034802.

[8] T. Okugi and W. Chou, eds., *Final focus system for linear colliders*, *ICFA Beam Dynamics Newsletter #61* (2013).

[9] R. Yang, A. Pastushenko, V. Cilento, K. Kubo, T. Naito, T. Okugi et al., *Momentum bandwidth of the KEK Accelerator Test Facility 2*, *Phys. Rev. Accel. Beams* **24** (2021) 051001.

[10] M. Pons, P. Bambade, A. Faus-Golfe, A. Latina and D. Schulte, *Comparison of ILC fast beam-beam feedback performance in the e^-e^- and e^+e^- modes of operation*, in *IEEE Particle Accelerator Conference*, Albuquerque, NM, U.S.A., 25–29 June 2007, pp. 2832–2834.

[11] L. Linssen, A. Miyamoto, M. Stanitzki and H. Weerts, eds., *Physics and Detectors at CLIC: CLIC Conceptual Design Report*, CERN-2012-003 [arXiv:1202.5940].

[12] A.W. Chao, K.H. Mess and M.T. andUniversi F. Zimmermann, *Handbook of Accelerator Physics and Engineering*, Second Edition, World Scientific Publishing (2012).

[13] R. Yang et al., *Tuning the ultralow β^* optics at the KEK Accelerator Test Facility 2*, *Phys. Rev. Accel. Beams* **23** (2020) 071003.

[14] M. Sands, *Emittance Growth from Radiation Fluctuations*, Tech. Rep., SLAC/AP-47 (1984).

[15] C.S. Hue, G.J. Cao, I.A. Andriyash, A. Knetsch, M.J. Hogan, E. Adli et al., *Efficiency and beam quality for positron acceleration in loaded plasma wakefields*, *Phys. Rev. Res.* **3** (2021) 043063.

[16] P. Chen, *Beamstrahlung and the QED, QCD backgrounds in linear colliders*, in proceedings of the *9th International Workshop on Photon-Photon Collisions*, San Diego, CA, U.S.A., 22–26 March 1992, 0418–429.

[17] A. Seryi, M. Woodley and P. Raimondi, *A Recipe for linear collider final focus system design*, *Conf. Proc. C* **030512** (2003) 2766.

[18] C.E. Doss et al., *Laser-ionized, beam-driven, underdense, passive thin plasma lens*, *Phys. Rev. Accel. Beams* **22** (2019) 111001.

[19] P. Chen, S. Rajagopalan and J.B. Rosenzweig, *Final Focusing and Enhanced Disruption From an Underdense Plasma Lens in a Linear Collider*, *Phys. Rev. D* **40** (1989) 923.

[20] P. Chen, K. Oide, A.M. Sessler and S.S. Yu, *Plasma based adiabatic Focuser*, *Phys. Rev. Lett.* **64** (1990) 1231.

[21] S. Diederichs, T.J. Mehrling, C. Benedetti, C.B. Schroeder, A. Knetsch, E. Esarey et al., *Positron transport and acceleration in beam-driven plasma wakefield accelerators using plasma columns*, *Phys. Rev. Accel. Beams* **22** (2019) 081301.

[22] S.Y. Kim, K. Moon, M. Chung, K.N. Sjobak, E. Adli, S. Doebert et al., *Witness electron beam injection using an active plasma lens for a proton beam-driven plasma wakefield accelerator*, *Phys. Rev. Accel. Beams* **24** (2021) 121304 [arXiv:2104.10288].

[23] J. van Tilborg et al., *Nonuniform discharge currents in active plasma lenses*, *Phys. Rev. Accel. Beams* **20** (2017) 032803.

[24] N.A. Bobrova, A.A. Esaulov, J.I. Sakai, P.V. Sasorov, D.J. Spence, A. Butler et al., *Simulations of a hydrogen-filled capillary discharge waveguide*, *Phys. Rev. E* **65** (2002) 016407.

[25] B.H.P. Broks, K. Garloff and J.J.A.M. van der Mullen, *Nonlocal-thermal-equilibrium model of a pulsed capillary discharge waveguide*, *Phys. Rev. E* **71** (2005) 016401.

[26] C.A. Lindstrøm et al., *Emittance Preservation in an Aberration-Free Active Plasma Lens*, *Phys. Rev. Lett.* **121** (2018) 194801 [*Erratum ibid.* **122** (2019) 129901] [arXiv:1808.03691].

[27] W.H. Bennett, *Magnetically Self-Focussing Streams*, *Phys. Rev.* **45** (1934) 890.

[28] B. Autin, H. Riege, E. Boggasch, K. Frank, L.D. Menna and G. Miano, *A Z-Pinch Plasma Lens for Focusing High-Energy Particles in an Accelerator*, *IEEE Trans. Plasma Sci.* **15** (1987) 226.

[29] J. Christiansen, K. Frank, H. Riege and R. Seeböck, *Studies of plasma lens with pseudo-spark geometry for application in high-energy particle accelerators*, Tech. Rep., CERN-PS-84-10-AA, CERN, Geneva (1984).

[30] E. Boggasch, J. Jacoby, H. Wahl, K.-G. Dietrich, D.H.H. Hoffmann, W. Laux et al., *z-pinch plasma lens focusing of a heavy-ion beam*, *Phys. Rev. Lett.* **66** (1991) 1705.

[31] C.A. Lindstrøm et al., *Emittance Preservation in an Aberration-Free Active Plasma Lens*, *Phys. Rev. Lett.* **121** (2018) 194801 [*Erratum ibid.* **122** (2019) 129901] [arXiv:1808.03691].

[32] K.N. Sjobak et al., *Strong focusing gradient in a linear active plasma lens*, *Phys. Rev. Accel. Beams* **24** (2021) 121306 [arXiv:2012.10680].

[33] C.A. Lindstrøm, *Staging of plasma-wakefield accelerators*, *Phys. Rev. Accel. Beams* **24** (2021) 014801 [arXiv:2007.05258].

[34] C.A. Lindstrøm and E. Adli, *Analytic plasma wakefield limits for active plasma lenses*, arXiv:1802.02750

[35] V. Yakimenko et al., *Prospect of Studying Nonperturbative QED with Beam-Beam Collisions*, *Phys. Rev. Lett.* **122** (2019) 190404 [arXiv:1807.09271].

[36] D. Schulte, *Study of electromagnetic and hadronic background in the interaction region of the TESLA collider*, Ph.D. thesis, Hamburg University (1997).

[37] T.O. Raubenheimer and F. Zimmermann, *Final focus systems in linear colliders*, *Rev. Mod. Phys.* **72** (2000) 95.

[38] K. Oide, *Synchrotron Radiation Limit on the Focusing of Electron Beams*, *Phys. Rev. Lett.* **61** (1988) 1713.

[39] K. Bane and G. Stupakov, *Dechirper Wakefields for Short Bunches*, *Nucl. Instrum. Meth. A* **820** (2016) 156 [arXiv:1601.07226].

[40] K. Oide, *Synchrotron Radiation Limit on the Focusing of Electron Beams*, *Phys. Rev. Lett.* **61** (1988) 1713.

[41] P. Chen, K. Oide, A.M. Sessler and S.S. Yu, *Plasma based adiabatic Focuser*, *Phys. Rev. Lett.* **64** (1990) 1231.